
A Bayesian Take on Gaussian Process Networks

Enrico Giudice

Dep. of Mathematics and Computer Science
University of Basel
Basel, Switzerland
enrico.giudice@unibas.ch

Jack Kuipers

Dep. of Biosystems Science and Engineering
ETH Zurich
Basel, Switzerland
jack.kuipers@bsse.ethz.ch

Giusi Moffa

Dep. of Mathematics and Computer Science, University of Basel, Basel, Switzerland
and Division of Psychiatry, University College London, London, UK
giusi.moffa@unibas.ch

Abstract

Gaussian Process Networks (GPNs) are a class of directed graphical models which employ Gaussian processes as priors for the conditional expectation of each variable given its parents in the network. The model allows describing continuous joint distributions in a compact but flexible manner with minimal parametric assumptions on the dependencies between variables. Bayesian structure learning of GPNs requires computing the posterior over graphs of the network and is computationally infeasible even in low dimensions. This work implements Monte Carlo and Markov Chain Monte Carlo methods to sample from the posterior distribution of network structures. As such, the approach follows the Bayesian paradigm, comparing models via their marginal likelihood and computing the posterior probability of the GPN features. Simulation studies show that our method outperforms state-of-the-art algorithms in recovering the graphical structure of the network and provides an accurate approximation of its posterior distribution.

1 Introduction

Bayesian networks (BNs) are a powerful tool for compactly representing joint distributions and the underlying relationships among a large set of variables [31]. These relationships are described via a directed acyclic graph (DAG), with each node in the graph representing a random variable. The joint distribution of a set of random variables $\mathbf{X} = \{X_1, \dots, X_n\}$ factorizes into conditional distributions for each variable given its parents in the DAG:

$$p(\mathbf{X}) = \prod_{i=1}^n p(X_i | \text{Pa}_{X_i}). \quad (1)$$

The DAG provides a visual description of the dependency structure among the variables, where missing edges encode conditional independence relations among pairs of variables. Thanks to their inherent flexibility and their ability to combine expert knowledge with data, Bayesian networks have been applied to a large range of domains [2]. More recently, Bayesian approaches have emerged to capture both network and parameter uncertainties across a variety of research areas [25, 1, 30].

In the absence of full prior knowledge of the underlying graph, inference on the structure is necessary. For this purpose, a plethora of *structure learning* algorithms have been proposed, which involve either learning the structure from the conditional independence relations in the data or assigning a score to each DAG and searching the graph space for high-scoring networks. An overview of

current algorithms and how they perform in benchmark studies is available [35], with hybrid methods combining both aspects offering the current state-of-the-art.

In this work, we focus on Bayesian methods, which sample DAGs according to their posterior distribution. Unlike approaches based on maximizing the score function, which return a single graph estimate, Bayesian approaches provide a full posterior distribution over DAGs, which we can use to make inference on the network’s features of interest. However, Bayesian structure inference typically requires a parametric model for the conditional distributions of each variable given its parents in the network to compute the posterior. Variations of the BDe score [21] are the usual choice for discrete-variable networks. Other information theory-based score functions [39, 3] are not Bayesian since they do not estimate a marginal likelihood but rather provide a measure of fitness of a DAG to the data based on the minimum description length principle.

For continuous-variable networks most of the current research has focused on the linear-Gaussian case, due to the availability of the closed-form BGe score [12, 24]. When relaxing the linear-Gaussian assumption, current approaches fall outside of the Bayesian framework since they do not target a posterior probability for DAGs but rather search the DAG space for a high-scoring network by minimizing a generic loss function. For example, Elidan [6] employs rank correlation as a goodness-of-fit measure between a graph and the observed data; Sharma and van Beek [38] propose modeling the relations among variables via regression splines and scoring the networks via a cross-validated score. Using the formulation by Zheng et al. [50] of the structure learning problem as a constrained continuous optimization, Yu et al. [49] model the conditional distributions via a graph neural network.

In this work, we develop a sampling scheme to perform fully Bayesian structure inference on generic continuous-variable networks with potentially non-linear relations among variables. We follow the strategy of Friedman and Nachman [9] and model the functional dependencies between each variable and its parents via Gaussian process priors. We extend their approach to the Bayesian framework by making structural inference based on the posterior distribution, which also involves treating the hyperparameters of the model as random. After a short review in Section 2 of Bayesian structure inference, Gaussian processes and how they can be used to parameterize BNs, Section 3 proposes a sampling scheme to perform fully Bayesian inference on nonlinear, continuous networks. In Sections 4 and 5 we evaluate and compare our algorithm to existing approaches on simulated and real data.

2 Background

2.1 Bayesian Structure Inference

When modelling a set of variables \mathbf{X} with a Bayesian network, a typical objective is to estimate the probability of a generic feature of interest Ψ . Examples of such a feature are the presence and direction of certain edges, the topological ordering of nodes or conditional independence relations among variables. Given a complete set D of observations of \mathbf{X} , we can obtain the posterior distribution of Ψ by integrating the probability or presence of the feature over the posterior distribution of graphs:

$$p(\Psi | D) = \sum_{\mathcal{G}} p(\Psi | \mathcal{G}) p(\mathcal{G} | D), \quad p(\mathcal{G} | D) \propto p(D | \mathcal{G}) p(\mathcal{G}), \quad (2)$$

wherein a key component is the likelihood of the data integrated over the prior distribution of the parameters θ of the conditional distributions:

$$p(D | \mathcal{G}) = \int p(D | \mathcal{G}, \theta) p(\theta | \mathcal{G}) d\theta. \quad (3)$$

The marginal likelihood $p(D | \mathcal{G})$ for a given DAG \mathcal{G} is available in closed form for specific combinations of priors on parameters and likelihood functions [11, 12].

The number of DAGs grows super-exponentially in the number of nodes [36], hence exact posterior inference is still exponentially complex making it effectively intractable for large networks [45]. Markov Chain Monte Carlo (MCMC) methods have successfully tackled the problem of posterior inference in the large and complex space of DAGs. The rationale consists in defining a Markov chain whose stationary distribution is the posterior distribution of interest $p(\mathcal{G} | D)$. Madigan et al. [28] suggested a Metropolis-Hastings sampler: at each step, the algorithm proposes a new DAG \mathcal{G}' and it accepts or rejects it according to a probability α . The value of α depends on the relative posterior

probability $p(\mathcal{G}' | D)$ of the proposal graph compared to that of the current DAG:

$$\alpha = \min \left\{ 1, \frac{p(\mathcal{G}' | D) Q(\mathcal{G}, \mathcal{G}')}{p(\mathcal{G} | D) Q(\mathcal{G}', \mathcal{G})} \right\} \quad (4)$$

where $Q(\cdot, \cdot)$ are the transition probabilities from one DAG to another. In its original formulation, the algorithm proposes a new graph by adding or deleting one edge from the current DAG, with Q uniformly distributed in the set of neighbouring DAGs (including the current one).

A number of refinements to the original method have been made over the years, providing for example more efficient proposal distributions [14, 20, 42]. The order MCMC approach by Friedman and Koller [8] introduced an important variation by sampling in the space of node orderings, which is smaller and smoother than the space of DAGs. Because of these attractive properties of the sample space, the order MCMC algorithm achieves superior mixing and convergence results compared to regular structure MCMC. Sampling orders however introduces a bias in the resulting posterior since node orders do not induce a uniform coverage in the DAG space [7]. The partition MCMC algorithm [23] corrects this bias in order MCMC by sampling in the larger space of ordered partitions of nodes to achieve unbiased samples from the posterior.

Current state-of-the-art methods rely on conditional independence tests to obtain a first coarse estimate of the structure to use as a starting point for a score-based method [46]. More sophisticated approaches involve iteratively expanding the search space to correct for errors in the initial estimate [26]. Such hybrid methods achieve efficient posterior inference [47, 26] in the selected search space by additionally precomputing all combinations of scores potentially needed in the chain so it can be run at a very low computational cost.

Key to enabling efficient DAG sampling is *decomposability*, a property ensuring that we can express the posterior probability of a DAG \mathcal{G} as a product of local scores that depend only on each variable and its parents in \mathcal{G} :

$$p(\mathcal{G} | D) = \prod_i^n S(X_i, \text{Pa}_{X_i}^{\mathcal{G}} | D). \quad (5)$$

Decomposability guarantees that we need to recompute only those scores whose parent sets have changed, or we can precompute all needed combinations of scores efficiently [26].

2.2 Gaussian Processes

Gaussian processes are a flexible tool used in machine learning for regression and classification tasks. Formally, a Gaussian Process (GP) is a distribution over functions such that every finite collection of its function values $\{f(x_1), f(x_2), \dots, f(x_k)\}$ has a multivariate Gaussian distribution [34]. A GP is therefore fully specified by its mean function $m(x) = \mathbb{E}[f(x)]$ and covariance function $k(x, x') = \text{Cov}[f(x), f(x')]$.

Due to their ability to model a large range of functional behaviours, GPs find common use as priors over regression functions $f(X) = \mathbb{E}(Y | X)$. A common GP regression model assumes independent Gaussian additive noise:

$$\begin{aligned} Y &= f(X) + \varepsilon \\ f(X) &\sim \text{GP}(0, k(x, x')) \\ \varepsilon &\sim \mathcal{N}(\mu, \sigma^2) \end{aligned} \quad (6)$$

Notably, GP models admit a closed-form expression of the marginal likelihood, in this case the likelihood of the N observations y marginalised over the prior distribution of f :

$$p(y) = (2\pi)^{-\frac{N}{2}} |K + \sigma^2 I|^{\frac{1}{2}} \exp \left(-\frac{1}{2} (y - \mu)^\top (K + \sigma^2 I)^{-1} (y - \mu) \right) \quad (7)$$

where K is the $N \times N$ Gram matrix $K_{ij} = k(x_i, x_j)$.

2.3 Gaussian Process Networks

Gaussian process networks (GPNs) refer to Bayesian networks whose conditional distributions are modelled via Gaussian process priors [9]. The structural equation model defining the distribution of

each variable X_i given its parents in a GPN is

$$X_i = f_i(\text{Pa}_{X_i}) + \varepsilon_i \quad (8)$$

where ε_i has a normal distribution $\mathcal{N}(\mu, \sigma^2)$ independent of the data and a Gaussian process prior is placed on the function f_i . Thanks to the nonparametric nature of GPs, the model in (8) can capture a wide range of functional dependencies between variables while maintaining the closed-form expression (7) for the marginal likelihood.

The covariance function k of the Gaussian process is typically parameterized by a set of hyperparameters θ which determine the behaviour of samples of f_i such as smoothness, shape or periodicity. When these hyperparameters (together with the noise mean μ and variance σ^2) are unknown they are typically learned by maximizing the marginal likelihood. Since the marginal likelihood and its derivatives are available in closed form, the optimization can be performed efficiently via gradient ascent [34]. The GPN model enables structure learning of networks on continuous variables without the need to make strict parametric assumptions on the distributions of the variables. In scenarios even with low sample sizes, Friedman and Nachman [9] have shown that searching for the highest-scoring structure can accurately reconstruct the underlying DAG under different functional relationships.

When estimating the score of a GPN, the common approach to learning the hyperparameters by simple maximization can however lead to problematic estimates, since many local optima may exist [4]. In addition, the resulting plug-in estimate of the marginal likelihood would not correctly reflect the uncertainty in the data of the full posterior. Bayesian model averaging provides a natural solution by integrating over the prior distribution of the hyperparameters to obtain a true marginal likelihood $p(D | \mathcal{G})$, which we can then use to perform posterior inference on the structure.

3 Bayesian Structure Inference for GPNs

In this section, we describe a method to sample from the posterior distribution of GPN DAG structures for continuous, non-linear data. To implement a fully Bayesian approach, we place priors over the hyperparameters θ of the kernel function and the Gaussian noise.

$$\begin{aligned} X &= f(\text{Pa}_X) + \varepsilon, \quad \varepsilon \sim \mathcal{N}(\mu, \sigma^2) \\ f &\sim \text{GP}(0, k_\theta(\cdot, \cdot)) \\ \theta &\sim \pi(\theta), \quad \mu, \sigma \sim \pi(\mu, \sigma). \end{aligned} \quad (9)$$

Let $\Theta = \{\mu, \sigma, \theta\}$ be the d -dimensional set of hyperparameters for a given node X and its parents Pa_X . Unless stated otherwise, throughout the rest of the text we assume a uniform prior over all structures $p(\mathcal{G}) \propto 1$. The score function is then the likelihood (7) of the observations x marginalized with respect to the hyperparameter priors:

$$S(X, \text{Pa}_X) = \int p(x | \text{Pa}_X, \Theta) \pi(\Theta | \text{Pa}_X) d\Theta. \quad (10)$$

If a variable X has no parents then the Gram matrix of the kernel is zero and the score function reduces to a Gaussian marginal likelihood. Since the above score function is generally intractable, one option is to use Monte Carlo (MC) approaches such as bridge sampling [29] to approximate it. Bridge sampling employs a Gaussian proposal distribution g and a bridge function h chosen to minimize the MSE of the resulting estimator. The bridge sampling estimator of (10) is then defined as

$$S(X, \text{Pa}_X) \approx \frac{\frac{1}{N_1} \sum_{i=1}^{N_1} p(x | \text{Pa}_X, \Theta_i) \pi(\Theta_i | \text{Pa}_X) h(\Theta_i | \text{Pa}_X)}{\frac{1}{N_2} \sum_{j=1}^{N_2} g(\Theta_j^* | \text{Pa}_X) h(\Theta_j^* | \text{Pa}_X)}, \quad (11)$$

$$\Theta_i \sim g(\Theta | \text{Pa}_X), \quad \Theta_j^* \sim p(\Theta | x, \text{Pa}_X), \quad i = 1, \dots, N_1, \quad j = 1, \dots, N_2.$$

The estimator is also a function of samples from the posterior of the hyperparameters $p(\Theta | x, \text{Pa}_X)$, which can easily be obtained via MCMC sampling. One can show that other approaches such as importance sampling or harmonic mean are special cases of bridge sampling [18]. MC methods based on bridge sampling provide asymptotically unbiased estimators for the marginal likelihood [48] but can become computationally expensive in high dimensions (i.e. for large parent sets).

Since sampling DAGs via MCMC requires computing a large number of scores of potential parent sets, which may not all be represented in the final sample, we avoid computing these expendable

Algorithm 1 GP network sampling scheme

Input Data D of n variables, feature of interest Ψ

Output Posterior probability of the feature $p(\Psi | D)$

- 1: **for** $i \in \{1, \dots, M\}$ **do**
 - 2: Sample DAG \mathcal{G}_i according to its Laplace approximate posterior $q(\mathcal{G}_i | D)$. \triangleright Eq. (12, 5)
 - 3: **for** $j \in \{1, \dots, n\}$ **do**
 - 4: Compute $S(X_j, \text{Pa}_{X_j}^{\mathcal{G}_i})$ via MC estimation. \triangleright Eq. (11)
 - 5: Compute posterior $p(\mathcal{G}_i | D)$. \triangleright Eq. (5)
 - 6: Compute posterior probability of Ψ via importance sampling. \triangleright Eq. (13)
-

scores by first running the MCMC algorithm using a Laplace approximation of the score (10) around the MAP value of Θ :

$$S_L(X, \text{Pa}_X) = p(x | \text{Pa}_X, \tilde{\Theta}) \pi(\tilde{\Theta} | \text{Pa}_X) \frac{(2\pi)^{d/2}}{|H|^{1/2}} \quad (12)$$

$$\text{with } \tilde{\Theta} = \underset{\Theta}{\operatorname{argmax}} p(x | \text{Pa}_X, \Theta) \pi(\Theta | \text{Pa}_X), \text{ and } H_{ij} = - \frac{\partial^2 p(x | \text{Pa}_X, \Theta) \pi(\Theta | \text{Pa}_X)}{\partial \Theta_i \partial \Theta_j} \Big|_{\Theta=\tilde{\Theta}}.$$

We denote the resulting posterior probability of a DAG \mathcal{G} from this Laplace approximated score as $q(\mathcal{G} | D)$ to distinguish it from the true posterior $p(\mathcal{G} | D)$.

The Laplace approximate score provides an approximation of the posterior at a lower computational cost, speeding up considerably the running time of the MCMC algorithm used to sample graphs. After sampling M graphs in the first step with the Laplace approximate score, we can make inference with respect to the true posterior by re-computing the scores and performing importance sampling. To estimate the posterior probability of a feature of interest Ψ via importance sampling we evaluate

$$p(\Psi | D) \approx \frac{\sum_{i=1}^M p(\Psi | \mathcal{G}_i) w_i}{\sum_{i=1}^M w_i}, \quad w_i = \frac{p(\mathcal{G}_i | D)}{q(\mathcal{G}_i | D)} \quad (13)$$

where $p(\mathcal{G}_i | D)$ and $q(\mathcal{G}_i | D)$ are the posterior probabilities of DAG \mathcal{G}_i computed respectively with the bridge sampling MC estimate (11) and the Laplace approximation (12) for the score. The procedure is summarized as pseudo-code in Algorithm 1.

Re-computing the score functions in a second step and implementing importance sampling is computationally advantageous compared to running the MCMC algorithm directly with the MC estimates of the scores. This advantage is simply due to the number of unique scores in the final chain being much lower than those evaluated or needed during the chain itself. Regardless of the MCMC algorithm used, we expect a substantial improvement in run-time compared to using the MC scores directly.

3.1 Implementation Details

Bayesian inference and optimization of the hyperparameters was performed via the Stan interface RStan [41]. The library offers a highly efficient C++ implementation of the No U-turn sampler [22], providing state-of-the-art posterior inference on the hyperparameters. We performed MC estimation of the marginal likelihood via the bridgesampling package [19], which can easily be combined with fitted Stan models.

In our implementation of Algorithm 1 we use order or partition MCMC to generate the network samples $q(\mathcal{G}_i | D)$; the procedure can however accommodate a variety of sampling methods, as long as they result in samples from the posterior. Given its good performance in benchmarking studies [35], we use the recent BiDAG [43] hybrid implementation for MCMC inference on the graph. The hybrid sampler requires an initial search space which is then improved upon to correct for possible estimation errors [26]. The initial search space is given in our case by the output of the dual PC algorithm [13]. For the bridge sampling estimator (11) of the marginal likelihood we used $N_1 = N_2 = 300$ particles from the proposal and posterior distribution over the hyperparameters. R code to implement Algorithm 1 and reproduce the results in Sections 4 and 5 is available at <https://github.com/enricogiudice/LearningGPNs>.

3.2 Score Equivalence

Unlike other score functions such as the BGe, the GP score does not satisfy score equivalence, meaning that DAGs belonging to the same Markov equivalence class may have different scores. Our method, therefore, generally differentiates models according to the direction of any of their edges. This appears to contradict the fact that any two DAGs within the same equivalence class are generally indistinguishable from observational data [32], since the joint distribution always factorizes according to either DAG. In the case of GPNs, however, an alternative factorization of a joint distribution generated by a given GPN may not have a representation that follows the structural equation model (8). The expression in equation (7) will therefore assign a higher likelihood to functional dependencies that can be expressed as the aforementioned model, due to the functions f_i being not generally invertible.

As demonstrated by Peters et al. [33], the asymmetry that allows distinguishing between Markov equivalent factorizations holds beyond the non-invertible case. Indeed, with the exception of the linear case, all structural models that take the additive form in (8) with Gaussian noise allow for the DAG to be identified beyond its Markov equivalence class. GPNs include cases where DAGs within an equivalence class are indistinguishable, such as when the functions f_i are linear. In this case, the computed scores of equivalent DAGs will be similar, as long as the GP prior allows learning sufficiently linear relations. Our numerical experiments, deferred to Section A.1 in the supplementary material, show that the GP-based score function automatically displays approximate score equivalent behaviour when learning data generated from a joint Gaussian distribution, which is coherent with the theoretical considerations of Peters et al. [33].

4 Experimental Results

We evaluate our Bayesian GP network inference scheme on data generated from known random networks with $n = 10$ nodes. The DAG structures are constructed from an Erdős-Rényi model, where each node has an independent probability of 0.2 to be connected with another with a higher topological ordering. For every node X_i in each randomly generated network, we then sample 100 observations as a non-linear function of its parents. The nonlinear data are generated by transforming the parents' instances using a weighted combination of six Fourier components

$$X_i = \sum_{Z \in \text{Pa}_{X_i}} \left\{ \sum_{j=0}^6 \beta_i v_{i,j} \sin(jZ) + \beta_i w_{i,j} \cos(jZ) \right\} + \epsilon_i. \quad (14)$$

The weights v_i and w_i are sampled from a Dirichlet distribution with concentration parameters equal to seven positive exponentially decreasing values $\gamma_k = e^{-k/\lambda}$, for $k = \{0, \dots, 6\}$. The parameter λ controls the rate of exponential decay, with values of λ close to zero providing mostly linear effects between variables and higher values resulting in increasingly non-linear relationships.

The edge coefficients β_i determine the strength of the dependencies between X_i and its parents and are sampled from a uniform distribution on $(\frac{1}{2}, 2)$; the noise variable ϵ_i has a standard normal distribution. Instances of root nodes (nodes without parents) are also sampled from a standard normal. The linear-Gaussian case corresponds asymptotically to $\lambda = 0$; in this case, we set the weights v_i and w_i to zero with the exception of $w_{i,0}$.

We compare all structure learning algorithms in terms of structural Hamming distance (SHD) [46], which compares estimated graphs \mathcal{G} with the ground truth graph \mathcal{G}^* . Following Lorch et al. [27], we compute the average SHD of the samples weighted by the posterior:

$$\mathbb{E}\text{-SHD}(p, \mathcal{G}^*) := \sum_{\mathcal{G}} \text{SHD}(\mathcal{G}, \mathcal{G}^*) p(\mathcal{G}|D). \quad (15)$$

The \mathbb{E} -SHD summarizes how close the estimated posterior is to the true DAG; it is however not a direct measure of the similarity of the estimated posterior to the true posterior.

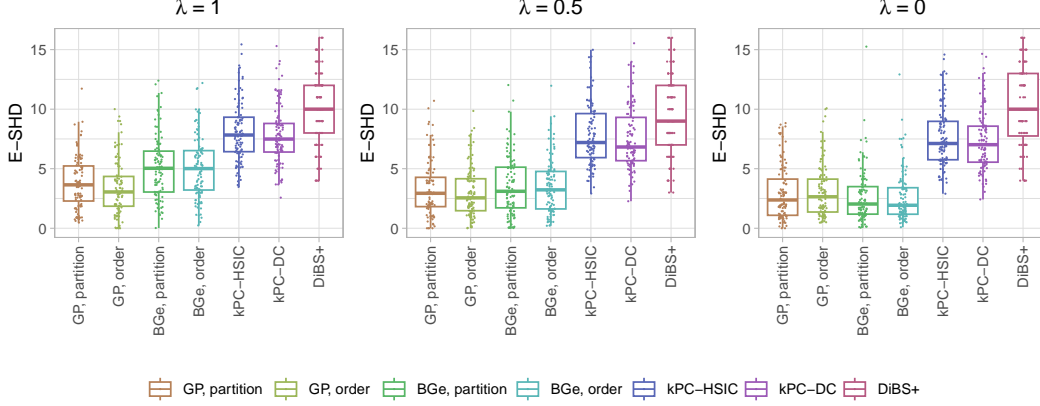


Figure 1: Distribution of \mathbb{E} -SHD values for all the different algorithms. $\lambda = 0$ corresponds to linear-Gaussian data while higher values increase the degree of non-linearity of the relations among variables.

4.1 Choice of Priors

Different choices of kernel for the GP prior result in different behaviours of the conditional expectation f in equation (9) of a variable X given its parents Pa_X . A simple model employs an additive kernel

$$k(\cdot, \cdot) = \sum_{i=1}^{|\text{Pa}_X|} k_{\theta_i}(\cdot, \cdot) \quad (16)$$

which corresponds to modeling each variable X as a sum of the individual contributions of each of its parents. The additive model serves to reduce the computational burden of calculating the scores by keeping the number of parameters as small as possible while preserving non-linearity in the model. Our approach can however easily accommodate more complex relationships at a higher computational cost, such as an additive kernel with all first-order interactions [5]:

$$k(\cdot, \cdot) = \tau_1 \sum_{i=1}^{|\text{Pa}_X|} k_{\theta_i}(\cdot, \cdot) + \tau_2 \sum_{i=1}^{|\text{Pa}_X|} \sum_{j=i+1}^{|\text{Pa}_X|} k_{\theta_i}(\cdot, \cdot) k_{\theta_j}(\cdot, \cdot). \quad (17)$$

For each parent $Z \equiv (\text{Pa}_X)_i$ we used a squared exponential kernel function $k_{\theta_i}(z, z') = \exp\left(-\frac{\|z - z'\|^2}{2\theta_i^2}\right)$, with each θ_i measuring the degree of non-linearity along the Z -th dimension. The kernel function has unit variance since the data are always normalized in the structure learning process. We assign the following independent prior distributions to the hyperparameter set $\Theta = \{\mu, \sigma, \theta_i : i \in 1, \dots, |\text{Pa}_X|\}$ of the GPN model (9):

$$\theta_i \sim \text{IG}(2, 2), \quad \mu \sim \mathcal{N}(0, 1), \quad \sigma \sim \text{IG}(1, 1). \quad (18)$$

The inverse-gamma priors for each lengthscale θ_i and the noise variance suppress values near zero, which in either case would result in overfitting and degenerate behaviour of samples of f [15]. The additional parameters τ_1 and τ_2 of the kernel function (17) were assigned independent $\text{IG}(1, 1)$ priors.

4.2 Results

We compare two different versions of our GP-based structure learning scheme: the first one employs the order MCMC algorithm for sampling DAGs, and the second uses partition MCMC. We then compare both versions of our GPN sampling scheme with order and partition MCMC with the BGe score [26]. To reduce the computational burden of the simulations, we employ the simpler additive kernel (16) for the GP score.

As an additional benchmark we include the DiBS+ algorithm [27], which models the adjacency matrix probabilistically, using particle variational inference to approximate a posterior over structures. In our simulations we parameterize DiBS+ by a neural network with one hidden layer with 5 nodes. We

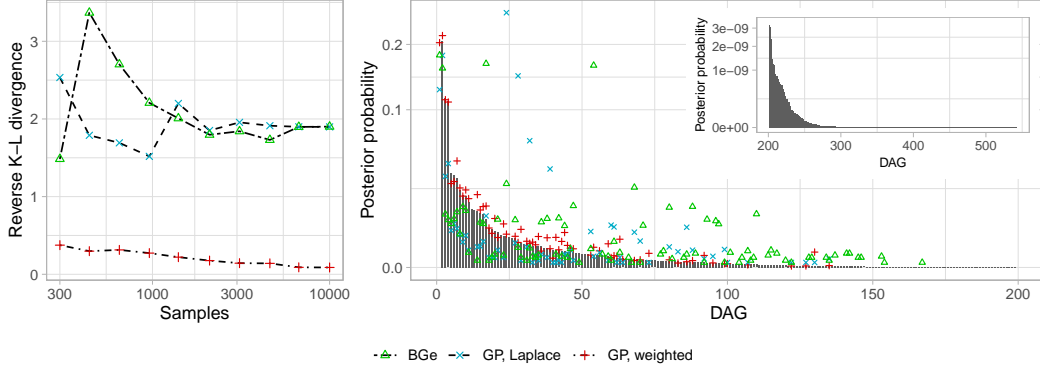


Figure 2: Left: reverse K-L divergence between the true posterior and the BGe posterior (green), the Laplace approximate posterior (blue) and the posterior obtained via importance sampling (red) as a function of the number of sampled DAGs. Right: the true posterior (gray) together with the BGe posterior (green), the Laplace approximate posterior (blue) and the posterior obtained via importance sampling (red). The majority of DAGs have a very low true posterior probability and are therefore never sampled by the MCMC algorithms (see inset).

also consider methods which rely on the constraint-based PC algorithm [40], which learns a network by testing for conditional independence among the variables. Since these are not Bayesian methods, we bootstrap the data to obtain different graph estimates via the PC algorithm [10]. To account for the non-linear dependencies between the variables we apply the kernel PC (kPC) algorithm [17] to the resampled data using two different independence tests: HSIC [16] and distance correlation [44].

Figure 1 shows, for three values of λ , the distribution of \mathbb{E} -SHD values for the different algorithms over the 100 generated structures. For non-linear data ($\lambda = 1$), both versions of the GP samplers outperform existing methods: the median \mathbb{E} -SHD for either of our algorithms is equal or lower than the bottom quartile of the BGe samplers. For linear ($\lambda = 0$) and slightly non-linear data ($\lambda = 0.5$), our GPN sampler performs competitively with the state-of-the-art BGe score-based sampling algorithms. All \mathbb{E} -SHD values are computed with respect to DAGs; the results comparing CPDAGs are available in figure A.4 in the supplementary material.

Besides estimating accurately the structure, our approach can quantify the uncertainty in its estimates via the sampled graphs from the posterior distribution over GPNs. In order to evaluate the accuracy of our sampling approach in estimating the general posterior over structures, we compare our estimated posterior distribution over DAGs with the “true” posterior, obtained by enumerating every possible structure and computing its score directly with equation (11). Due to the exceedingly large number of DAGs, this approach is only feasible with small structures. The left panel of figure 2 shows the reverse Kullback-Leibler (K-L) divergence between the estimated and true posteriors for a given network with $n = 4$ nodes, as a function of the number of samples M in the partition MCMC algorithm. The estimated (“GP, weighted”) posterior probability $p(\mathcal{G} | D)$ for a generic DAG \mathcal{G} is obtained by setting $p(\Psi | \mathcal{G}_i) = \mathbb{1}_{(\mathcal{G}_i = \mathcal{G})}$ in equation (13). Reverse K-L divergence was chosen as a metric since the algorithms assign a probability of zero to DAGs that were not sampled.

The plot includes the divergence between the Laplace approximate posterior $q(\mathcal{G} | D)$ in equation (13) and the true posterior, as well as between the posterior obtained with the BGe score and the true posterior. The divergence of the Laplace approximation is reduced by roughly one order of magnitude by weighting the samples via importance sampling. For reference, the DiBS+ algorithm yields a reverse K-L divergence of 27.8 with 1000 samples, i.e. two orders of magnitude higher than our approach, despite also being allocated longer run-times (see supplementary material). Sampling a higher number of graphs with DiBS+ quickly becomes infeasible since its run-time scales quadratically with the number of samples [27], while MCMC sampling scales linearly with M . The right panel of figure 2 shows the posterior distributions over the 543 possible DAGs, for $M = 10^4$, obtained after complete enumeration and by sampling with different methods. The plots confirm that as the number of sampled DAGs increase our approach can accurately reflect the full posterior uncertainty. The results also underline the importance of sampling from the hyperparameters’ priors in order to obtain an accurate representation of the posterior, as the Laplace approximation of the

Table 1: Performance of the different algorithms in reconstructing the consensus network from flow cytometry data. The last two columns show the posterior probabilities of the two features experimentally validated by Sachs et al. [37], where the edge on the left should be present and the one on the right absent; higher probabilities for both columns are better.

	\mathbb{E} -SHD	\mathbb{E} -TP	\mathbb{E} -FP	Erk \rightarrow Akt	Erk \nrightarrow PKA
GP, partition	14.5	7.2	4.7	1	0.75
GP, order	14.6	6.8	4.4	1	0.42
GP ² , partition	16.7	6.6	6.3	1	0
GP ² , order	16.7	6.7	6.4	1	0.34
BGe, partition	15.9	4.3	3.2	0	1
BGe, order	15.3	4.4	2.7	0.17	0.98
kPC-HSIC	17	5.5	5.5	0.69	0.26
kPC-DC	16.9	6	5.8	0.72	0.28
DiBS+	16.1	5	4.2	0.45	0.7

marginal likelihood results in a highly biased approximation even when sampling a large number of DAGs.

5 Application on Protein Signaling Networks

We also applied our GP score-based structure inference to the flow cytometry dataset of Sachs et al. [37] to learn protein signaling pathways. The authors provide an accepted consensus network, which we used as our reference. We considered the first experimental condition, consisting of 853 single-cell observations of $n = 11$ phosphoproteins and phospholipids in human T cells. The first three columns of table 1 shows the performances of all the different algorithms in reconstructing the consensus network. The results include the GP model using the additive kernel (17) with all first-order interactions, denoted as GP². We measure the different algorithms in terms of the \mathbb{E} -SHD, as well as the \mathbb{E} -TP and \mathbb{E} -FP, the absolute number of TP and FP edges in the DAGs weighted by the posterior, obtained by replacing the SHD in equation (15) by TP or FP, respectively.

One of the benefits of Bayesian structure inference is the possibility of deriving posterior probabilities of specific edges of interest in the network. In their work, Sachs et al. [37] experimentally tested two relationships between the proteins by intervening directly on the cells. By means of small interfering RNA inhibition, they concluded that the inhibition of Ekt has a direct effect on Akt, while there was a weaker and non-significant effect on PKA. We therefore expect an edge $\text{Erk} \rightarrow \text{Akt}$ but no directed edge (or path) from Erk to PKA in the learned networks. The last two columns of table 1 display the posterior probabilities of these two features according to the different algorithms. GP- and BGe-based methods perform best, with our GP learner correctly assigning the highest probability to the edge $\text{Erk} \rightarrow \text{Akt}$, while the lack of the edge Erk to PKA is predicted with a lower probability. The sparser BGe score-based methods assign a lower probability to the first edge, but correctly predict the absence of the second edge.

6 Conclusions

In this work we have proposed a procedure that efficiently performs Bayesian structural inference on Gaussian process networks and estimate the posterior of generic features of interest. Building on the original GPN idea by Friedman and Nachman [9], we now embed it in a fully Bayesian framework. In particular, our approach involves placing priors on the hyperparameters of the score function and sampling DAGs via MCMC. Although more computationally expensive than a greedy search over the DAG space for a high-scoring network, the Bayesian approach allows one to accurately quantify the uncertainty in features of the network. This is made feasible by minimizing the number of scores to compute in a MCMC chain via importance sampling, as well as harnessing the advances in MC and MCMC methods [19, 26, 41, 43] that have been made since the introduction of GP networks.

The flexible nature of GPs allows the corresponding BNs to model a large range of functional dependencies between continuous variables. In the case of linear dependencies, our method remains

competitive with state-of-the-art methods and exhibits desirable properties such as (approximate) score equivalence. The versatility of the model is particularly useful in domains where the nature of relations among variables in unknown and strict parametric assumptions on the distributions of the variables want to be avoided. Based on the promising simulation results and the convenient properties of our method, we believe that it holds potential for making accurate inference on the underlying structure of BNs in complex domains.

References

- [1] Federico Castelletti and Guido Consonni. Discovering causal structures in Bayesian Gaussian directed acyclic graph models. *Journal of the Royal Statistical Society: Series A (Statistics in Society)*, 183:1727–1745, 2020.
- [2] Rónán Daly, Qiang Shen, and Stuart Aitken. Learning Bayesian networks: approaches and issues. *The Knowledge Engineering Review*, 26:99–157, 2011.
- [3] Luis M. de Campos. A scoring function for learning Bayesian networks based on mutual information and conditional independence tests. *Journal of Machine Learning Research*, 7: 2149–2187, 2006.
- [4] David Duvenaud, James Lloyd, Roger Grosse, Joshua Tenenbaum, and Ghahramani Zoubin. Structure discovery in nonparametric regression through compositional kernel search. In *Proceedings of the 30th International Conference on Machine Learning*, volume 28, pages 1166–1174, 2013.
- [5] David K. Duvenaud, Hannes Nickisch, and Carl Rasmussen. Additive Gaussian processes. In *Advances in Neural Information Processing Systems*, volume 24, pages 226–234, 2011.
- [6] Gal Elidan. Lightning-speed structure learning of nonlinear continuous networks. In *Proceedings of the Fifteenth International Conference on Artificial Intelligence and Statistics*, volume 22, pages 355–363, 2012.
- [7] Byron Ellis and Wing Hung Wong. Learning causal Bayesian network structures from experimental data. *Journal of the American Statistical Association*, 103:778–789, 2008.
- [8] Nir Friedman and Daphne Koller. Being Bayesian about network structure: a Bayesian approach to structure discovery in Bayesian networks. *Machine Learning*, 50:95–125, 2003.
- [9] Nir Friedman and Iftach Nachman. Gaussian process networks. In *Proceedings of the Sixteenth Conference on Uncertainty in Artificial Intelligence*, pages 211–219, 2000.
- [10] Nir Friedman, Moises Goldszmidt, and Abraham Wyner. Data analysis with Bayesian networks: a bootstrap approach. In *Proceedings of the Fifteenth Conference on Uncertainty in Artificial Intelligence*, pages 196–205, 2013.
- [11] Dan Geiger and David Heckerman. Learning Gaussian networks. In *Proceedings of the Tenth Conference on Uncertainty in Artificial Intelligence*, pages 235–243, 1994.
- [12] Dan Geiger and David Heckerman. Parameter priors for directed acyclic graphical models and the characterization of several probability distributions. *The Annals of Statistics*, 30:1412–1440, 2002.
- [13] Enrico Giudice, Jack Kuipers, and Giusi Moffa. The dual PC algorithm for structure learning. In *Proceedings of the 11th International Conference on Probabilistic Graphical Models*, volume 186, pages 301–312, 2022.
- [14] Paolo Giudici and Robert Castelo. Improving Markov chain Monte Carlo model search for data mining. *Machine Learning*, 50:127–158, 2003.
- [15] Robert B. Gramacy and Herbert K. H. Lee. Bayesian treed Gaussian process models with an application to computer modeling. *Journal of the American Statistical Association*, 103: 1119–1130, 2008.

- [16] Arthur Gretton, Kenji Fukumizu, Choon Teo, Le Song, Bernhard Schölkopf, and Alex Smola. A kernel statistical test of independence. In *Advances in Neural Information Processing Systems*, volume 20, pages 585–592, 2007.
- [17] Arthur Gretton, Peter Spirtes, and Robert Tillman. Nonlinear directed acyclic structure learning with weakly additive noise models. In *Advances in Neural Information Processing Systems*, volume 22, pages 1847–1855, 2009.
- [18] Quentin F. Gronau, Alexandra Sarafoglou, Dora Matzke, Alexander Ly, Udo Boehm, Maarten Marsman, David S. Leslie, Jonathan J. Forster, Eric-Jan Wagenmakers, and Helen Steingroever. A tutorial on bridge sampling. *Journal of Mathematical Psychology*, 81:80–97, 2017.
- [19] Quentin F. Gronau, Henrik Singmann, and Eric-Jan Wagenmakers. Bridgesampling: An R package for estimating normalizing constants. *Journal of Statistical Software*, 92:1–29, 2020.
- [20] Marco Grzegorzczak and Dirk Husmeier. Improving the structure MCMC sampler for Bayesian networks by introducing a new edge reversal move. *Machine Learning*, 71:265–305, 2008.
- [21] David Heckerman and Dan Geiger. Learning Bayesian networks: a unification for discrete and Gaussian domains. *Proceedings of the Eleventh Conference on Uncertainty in Artificial Intelligence*, pages 274–284, 1995.
- [22] Matthew D. Homan and Andrew Gelman. The No-U-turn sampler: adaptively setting path lengths in Hamiltonian Monte Carlo. *Journal of Machine Learning Research*, 15:1593–1623, 2014.
- [23] Jack Kuipers and Giusi Moffa. Partition MCMC for inference on acyclic digraphs. *Journal of the American Statistical Association*, 112:282–299, 2017.
- [24] Jack Kuipers, Giusi Moffa, and David Heckerman. Addendum on the scoring of Gaussian directed acyclic graphical models. *The Annals of Statistics*, 42:1689–1691, 2014.
- [25] Jack Kuipers, Thomas Thurnherr, Giusi Moffa, Polina Suter, Jonas Behr, Ryan Goosen, Gerhard Christofori, and Niko Beerenwinkel. Mutational interactions define novel cancer subgroups. *Nature Communications*, 9:4353, 2018.
- [26] Jack Kuipers, Polina Suter, and Giusi Moffa. Efficient sampling and structure learning of Bayesian networks. *Journal of Computational and Graphical Statistics*, 31:639–650, 2022.
- [27] Lars Lorch, Jonas Rothfuss, Bernhard Schölkopf, and Andreas Krause. DiBS: differentiable Bayesian structure learning. In *Advances in Neural Information Processing Systems*, volume 34, pages 24111–24123, 2021.
- [28] David Madigan, Jeremy York, and Denis Allard. Bayesian graphical models for discrete data. *International Statistical Review*, 63:215–232, 1995.
- [29] Xiao-Li Meng and Wing Hung Wong. Simulating ratios of normalizing constants via a simple identity: a theoretical exploration. *Statistica Sinica*, 6:831–860, 1996.
- [30] Giusi Moffa, Jack Kuipers, Giuseppe Carrà, Cristina Crocamo, Elizabeth Kuipers, Matthias Angermeyer, Traolach Brugha, Mondher Toumi, and Paul Bebbington. Longitudinal symptomatic interactions in long-standing schizophrenia: a novel five-point analysis based on directed acyclic graphs. *Psychological Medicine*, pages 1–8, 2021.
- [31] Judea Pearl. *Probabilistic reasoning in intelligent systems: networks of plausible inference*. Morgan Kaufmann Publishers Inc., 1988.
- [32] Judea Pearl. *Causality: Models, reasoning, and inference*. Cambridge University Press, 2000.
- [33] Jonas Peters, Joris Mooij, Dominik Janzing, and Bernhard Schölkopf. Causal discovery with continuous additive noise models. *Journal of Machine Learning Research*, 15:2009–2053, 2013.
- [34] Carl Edward Rasmussen. *Gaussian processes in machine learning*. Springer Berlin Heidelberg, 2004.

- [35] Felix L. Rios, Giusi Moffa, and Jack Kuipers. Benchpress: a scalable and platform-independent workflow for benchmarking structure learning algorithms for graphical models. *arXiv:2107.03863*, 2021.
- [36] Robert W. Robinson. Counting labeled acyclic digraphs. In *New Directions in Graph Theory*, pages 239–273. New York: Academic Press, 1973.
- [37] Karen Sachs, Omar Perez, Dana Pe’er, Douglas A. Lauffenburger, and Garry P. Nolan. Causal protein-signaling networks derived from multiparameter single-cell data. *Science*, 308:523–529, 2005.
- [38] Charupriya Sharma and Peter van Beek. Scalable Bayesian network structure learning with splines. In *Proceedings of The 11th International Conference on Probabilistic Graphical Models*, volume 186, pages 181–192, 2022.
- [39] Tomi Silander, Teemu Roos, and Petri Myllymäki. Locally minimax optimal predictive modeling with Bayesian networks. In *Proceedings of the Twelfth International Conference on Artificial Intelligence and Statistics*, volume 5, pages 504–511, 2009.
- [40] Peter Spirtes, Clark Glymour, and Richard Scheines. *Causation, prediction, and search*. Springer New York, NY, 1993.
- [41] Stan Development Team. RStan: the R interface to Stan, R package version 2.21.8, 2023. URL <https://mc-stan.org/>.
- [42] Chengwei Su and Mark E. Borsuk. Improving structure MCMC for Bayesian networks through Markov blanket resampling. *Journal of Machine Learning Research*, 17:1–20, 2016.
- [43] Polina Suter, Jack Kuipers, Giusi Moffa, and Niko Beerenwinkel. Bayesian structure learning and sampling of Bayesian networks with the R package BiDAG. *Journal of Statistical Software*, 105:1–31, 2023.
- [44] Gábor J. Székely, Maria L. Rizzo, and Nail K. Bakirov. Measuring and testing dependence by correlation of distances. *The Annals of Statistics*, 35:2769–2794, 2007.
- [45] Topi Talvitie, Aleksis Vuoksenmaa, and Mikko Koivisto. Exact sampling of directed acyclic graphs from modular distributions. In *Proceedings of The 35th Uncertainty in Artificial Intelligence Conference*, pages 965–974, 2020.
- [46] Ioannis Tsamardinos, Laura Brown, and Constantin Aliferis. The max-min hill-climbing Bayesian network structure learning algorithm. *Machine Learning*, 65:31–78, 2006.
- [47] Jussi Viinikka, Antti Hyttinen, Johan Pensar, and Mikko Koivisto. Towards scalable Bayesian learning of causal DAGs. In *Advances in Neural Information Processing Systems*, volume 33, pages 6584–6594, 2020.
- [48] Jackie S.T. Wong, Jonathan J. Forster, and Peter W.F. Smith. Properties of the bridge sampler with a focus on splitting the MCMC sample. *Statistics and Computing*, 30:799–816, 2020.
- [49] Yue Yu, Jie Chen, Tian Gao, and Mo Yu. DAG-GNN: DAG structure learning with graph neural networks. In *Proceedings of the 36th International Conference on Machine Learning*, volume 97, pages 7154–7163, 2019.
- [50] Xun Zheng, Bryon Aragam, Pradeep K. Ravikumar, and Eric P. Xing. DAGs with NO TEARS: continuous optimization for structure learning. In *Advances in Neural Information Processing Systems*, volume 31, pages 9492–9503, 2018.

A Supplementary Material

A.1 Measuring Score Equivalence

In this section we perform a simulation study to measure the degree to which the GP score is capable of inferring the correct direction of the edges in the graph. Following the considerations of Section 3.2, the aim of the experiment is to gauge to what degree the model is able to correctly identify edge directions for non-linear data while retaining score equivalence in the linear-Gaussian case.

We generate 100 observations following the approach outlined in Section 4 from a “forward” network consisting of a chain of 5 nodes $X_1 \rightarrow \dots \rightarrow X_5$. We then compare the score of the forward network with that of a “backward” network, which has all edges reversed. In figure A.1 we then plot the difference in log-score between the forward and backward models as a function of the non-linearity parameter λ . For each value of λ , the log-difference in scores was averaged over 100 runs.

The results show that for roughly linear-Gaussian relationships ($\lambda \approx 0$), score equivalence of the Bayesian GP score holds in expectation, while for larger deviations from the linear-Gaussian model, the score increasingly favors the correct forward DAG. For $\lambda = 0.75$, the score of the forward model is greater than that of the backward model in more than 90% of the simulations.

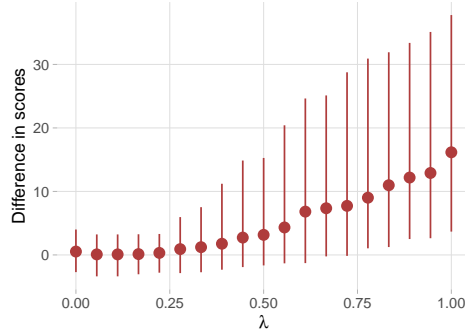


Figure A.1: The median difference in GP log score between the forward and backward model, with 0.1- and 0.9-quantiles.

A.2 Additional Simulation Results

Further to the results in Section 4.2 of the main text, here we present additional metrics comparing the various algorithms’ performances. We construct ROC-like curves counting the average number of true negative (TN) and false positive (FP) edges of the highest scoring graph. We define the true positive edge rate and a modified false positive edge rate as

$$\text{TPR} = \frac{\text{TP}}{\text{P}} \quad \text{FPRp} = \frac{\text{FP}}{\text{P}}. \quad (19)$$

We scale the FPs by the number of positives to obtain measures on a similar scale, since the number of true negative edges can be exceedingly large for DAGs. Different points in the ROC space are produced by varying the hyperparameters of the different structure learning algorithms; the process also allows tuning the hyperparameters of each algorithm to minimize their \mathbb{E} -SHD.

Figure A.2 displays the TPR and FPRp for different values of the hyperparameters for a selection of the considered algorithms. For the kPC algorithm-based methods we vary the parameter controlling the type I error; for the BGe score-based methods we vary the prior on the precision matrix of the Gaussian likelihood. Since the GP score-based algorithms do not rely on any hyperparameters that directly control the sparsity of the resulting graphs, we simply penalize the number of edges in the DAGs via a prior on the graph space. The prior depends on the number of edges according to the following distribution: $p(\mathcal{G}) \propto \exp\{-\gamma \#(\text{edges})\}$. The ROC-like curves are then constructed by averaging the TPR and FPRp over the 100 runs for each value of the hyperparameters, under the

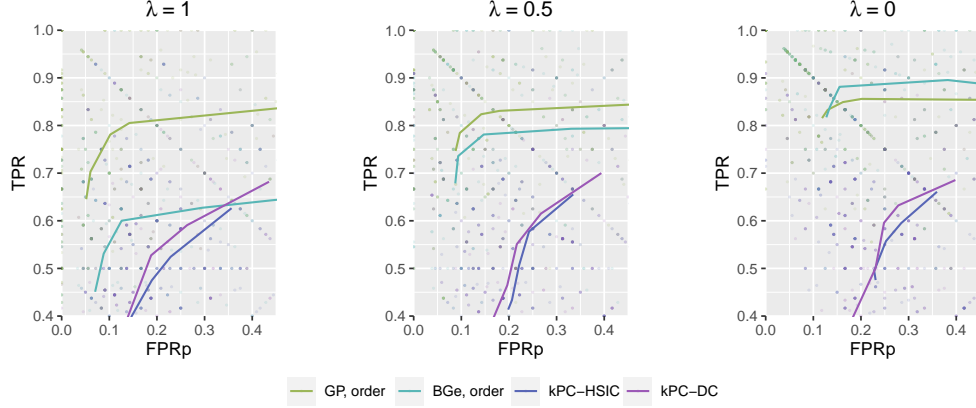


Figure A.2: Average FPRp and TPR values for a selection of the different algorithms. $\lambda = 0$ corresponds to linear-Gaussian data while higher values increase the degree of non-linearity of the relations among variables.

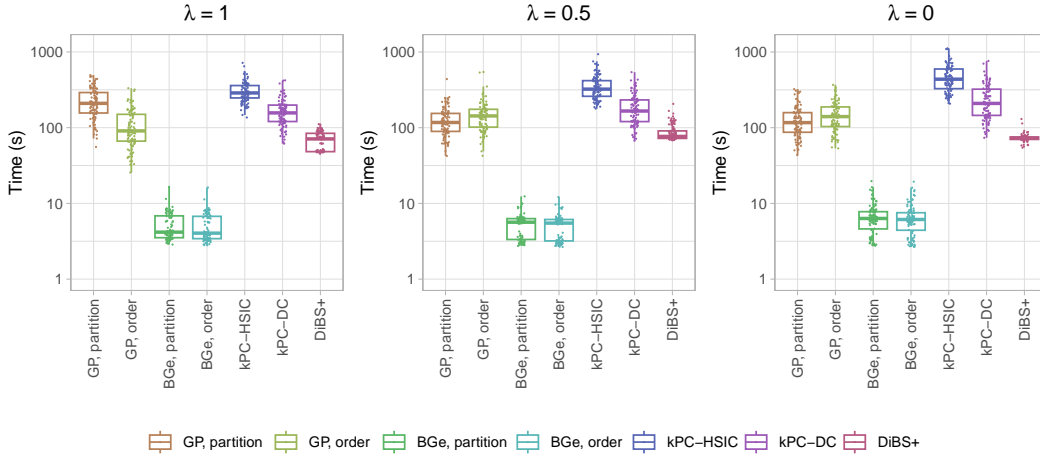


Figure A.3: Distribution of run-times for all the different algorithms. $\lambda = 0$ corresponds to linear-Gaussian data while higher values increase the degree of non-linearity of the relations among variables.

settings described in Section 4. The partition MCMC results are omitted since they are in very close agreement with the output of order MCMC.

According to the ROC-like curves, the two BGe score-based methods perform only slightly better than the GP-based methods for linear data; in all other cases, our methods achieve both higher TPR values and lower FPRp values compared to all the other benchmarks. The value of the hyperparameters that minimized the \mathbb{E} -SHD of each algorithm was used to obtain the plots in figure 1 of the main text.

Figure A.3 displays the run-times of the different methods needed to generate figure 1. The run-times are stable across the different levels of non-linearity parameterized by λ , with the k-PC algorithms being the most computationally expensive, followed by our GP score-based approach, DiBS+ and finally the BGe score-based MCMC methods which are the fastest.

Figure A.4 shows the distribution of \mathbb{E} -SHD values computed with respect to the true and estimated CPDAGs for the same experiments in figure 1; the results are in line with those comparing the DAGs. Cyclic graphs occasionally returned by DiBS+ were discarded.

We performed an additional experiment comparing the ability of the different methods to model the posterior distribution over DAGs as a function of their run-time. Figure A.5 shows the reverse K-L divergence between the “true” posterior (obtained by enumerating every possible structure and

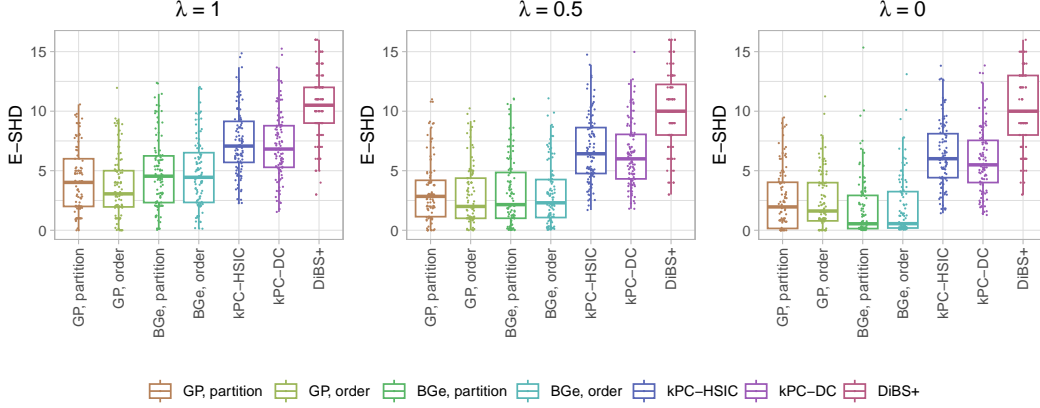


Figure A.4: Distribution of \mathbb{E} -SHD values comparing the true and estimated CPDAGs. $\lambda = 0$ corresponds to linear-Gaussian data while higher values increase the degree of non-linearity of the relations among variables.

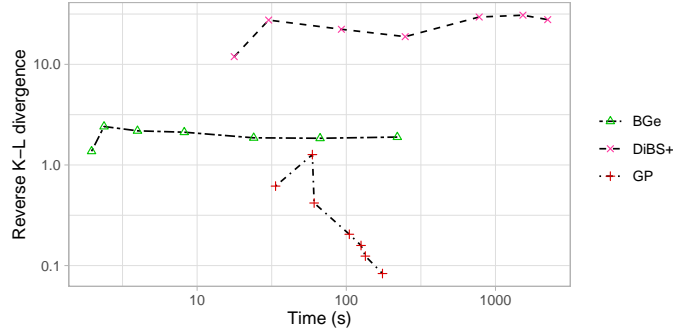


Figure A.5: Reverse K-L divergence between the true posterior and the BGe posterior (green), DiBS+ (pink) and the posterior obtained via our GP score-based approach (red) as a function of run-time.

computing the score of the GPN via bridge sampling) and the posteriors estimated with the different methods. We used the same 4-node DAG of figure 2, and the different run-times were obtained by increasing the number of samples taken from the posterior for each method. Three methods are compared: partition MCMC with the BGe score, DiBS+ and our approach of using partition MCMC with the GP score together with importance sampling.

The results show that as the number of sampled DAGs increase, our GP-based method is able to successfully represent the posterior distribution. The BGe score-based approach and DiBS+ are not however able to reach low K-L values, even as the number of samples is increased and the methods are given additional run-time.

Finally, we repeated the simulations outlined in Section 4 on larger randomly generated DAGs with $n = 15$ nodes. Figures A.6 and A.7 show the distribution of \mathbb{E} -SHD values computed respectively with respect to DAGs and CPDAGs. Figure A.8 shows the corresponding run-times needed to run each algorithm. The relative performance of the different methods does not differ compared to the results with lower-dimensional networks.

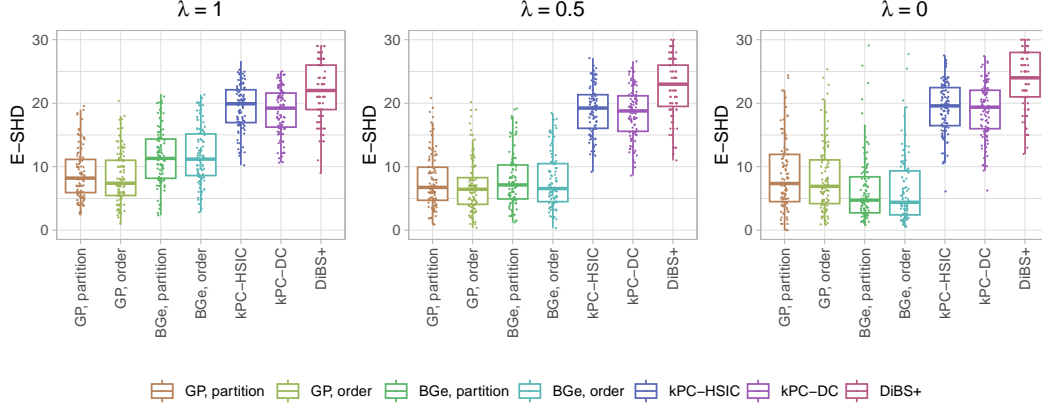


Figure A.6: Distribution of \mathbb{E} -SHD for networks with $n = 15$ nodes, computed on the DAG space. $\lambda = 0$ corresponds to linear-Gaussian data while higher values increase the degree of non-linearity of the relations among variables.

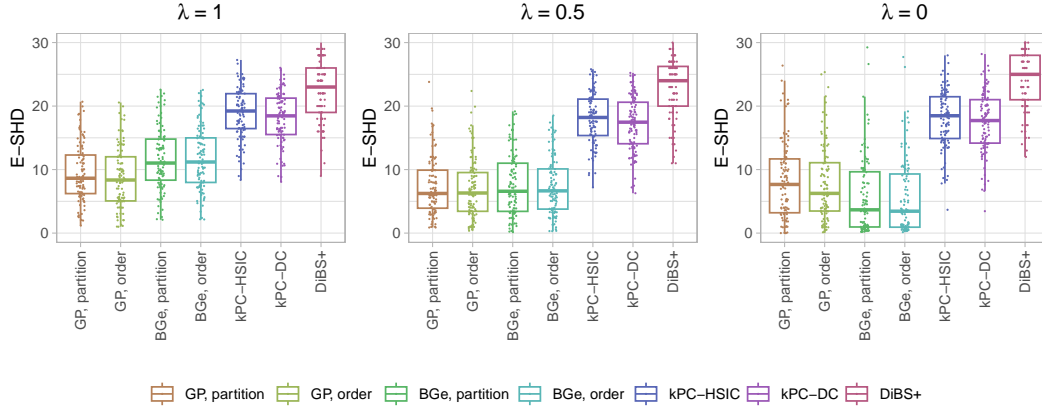


Figure A.7: Distribution of \mathbb{E} -SHD for networks with $n = 15$ nodes, computed on the CPDAG space. $\lambda = 0$ corresponds to linear-Gaussian data while higher values increase the degree of non-linearity of the relations among variables.

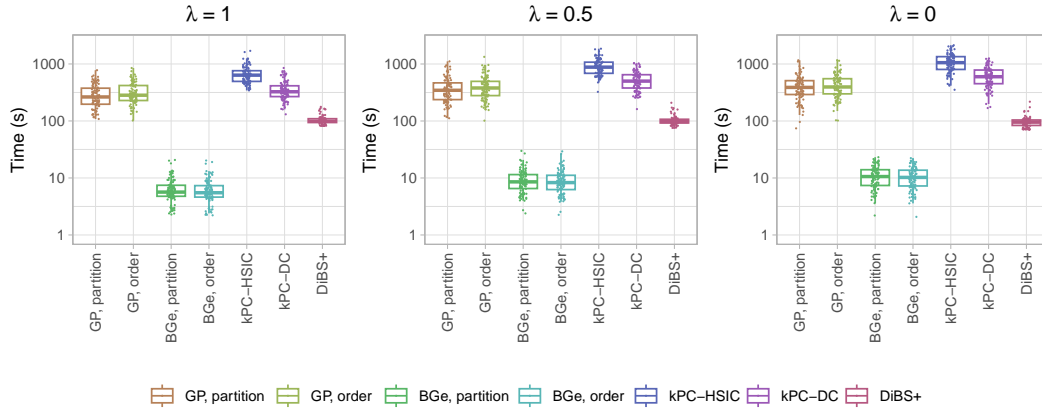


Figure A.8: Distribution of run-times for networks with $n = 15$ nodes. $\lambda = 0$ corresponds to linear-Gaussian data while higher values increase the degree of non-linearity of the relations among variables.